Tetrapods based Engineering of Organic Phase Change Material for Thermal Energy Storage

Kalidasan Balasubramanian [a], Adarsh Kumar Pandey [a*], Reza Abolhassani [b], Horst-Günter Rubahn [b], Saidur Rahman [a], Yogendra Kumar Mishra [b]

[a)] *Research Centre for Nano-Materials and Energy Technology (RCNMET), School of Engineering and Technology, Sunway University, No. 5, Jalan Universiti, Bandar Sunway, Petaling Jaya, 47500 Selangor Darul Ehsan, Malaysia.*

[b)] *Mads Clausen Institute, NanoSYD, University of Southern Denmark, Alsion 2, 6400, Sønderborg, Denmark*

ABSTRACT

Phase change materials (PCM) are largely assessed on their ability towards energy storage and their enthalpy efficiency of discharging the stored energy. Nevertheless, their applications are limited by the low thermal conductivity behaviour, despite their tunable transition temperature abilities. The present work demonstrates a novel concept to develop and explore PCM composite by embedding two unique zinc oxide tetrapod classes to engineer the heat transfer mechanism for potential utilization in thermal energy storage. Tetrapods embedded phase change material (TPCM) composite displayed up to 94% enhancement in thermal conductivity without compromising melting enthalpy. TPCM composite with high thermal conductivity, high heat capacity, broad photo-absorptivity, improved stability in isothermal conditions, and long thermal cycles offer attractive solutions for effective thermal energy storage, efficient solar energy harnessing, and thermal management. With demonstrated abilities, the developed TPCM composite material could play a significant role in the progress of renewable energy needs in future.

Keywords: Energy harnessing; zinc oxide tetrapods; phase change material; composite; thermal energy storage.

[*] Correspondence: adarshp@sunway.edu.my (A.K. Pandey);

Graphical Abstract

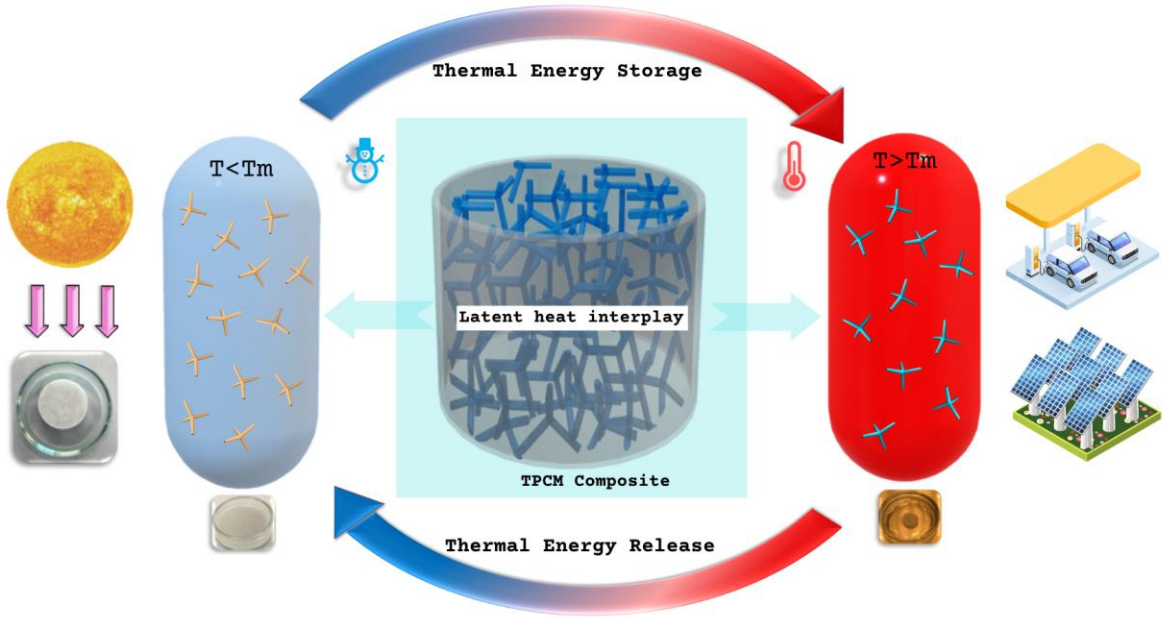

1.0 INTRODUCTION

Remarkable growth and development in industrialization and technologies have been highly operative with a continuous supply of electric power. Huge consumption of conventional energy for electricity generation has led to several global, environmental and socio-economic problems. Among the total consumed industrial energy sources, almost 20-30% remains unutilized in the form of waste heat energy. Amid the waste heat, around 65% of the wasted heat energy is discharged at the temperature of 100 °C into the surrounding atmosphere[1]. Low grade heat energy released to the atmosphere not only raises the ambient temperature but also disrupts the comfortable living conditions. Up to now, almost no cost effective techniques are available to harness the 30% of waste heat released from the industries. Based on the many existing research works and surveys, it's quite obvious that the only solution for bridging the huge demand-supply chain of energy in an environmentally friendly way, is through deeper penetration of renewable energy resources in scalable, economical, reliable and sustainable energy storage units[2]. Just having one excellent energy storage unit won't be an effective solution to meet the diverse energy demands. Therefore, various energy storage techniques like mechanical, electrical, chemical, electrochemical, and thermal systems are under immense investigation[3]. Performance of thermal storage media are mainly evaluated on the basis of operating temperature (°C), energy density (MJ/m^3), and heat storage enthalpy (J/g)[4]. Thermophysical and thermochemical storages are the major classification of thermal storage media. Use of the thermophysical storage techniques in the form of phase change materials (PCM) for thermal energy storage (TES) is very cost effective and efficient as compared to the 2% efficiency of thermoelectric generators[5]. The thermophysical energies are mainly stored in the form of sensible heat (varying temperature, single phase) and latent heat (constant temperature, dual phase)[6]. The phase change materials (PCMs) are of great interest with respect to TES because heat transfer in PCMs could be realized from molecular level to real time applications. The PCMs are actively being used in building[7], solar thermal systems[8], photovoltaic thermal units[9], textile garments[10], battery thermal management[11], microelectronics[12], food storage and transportations[13], pharmaceutical, aerospace, and in many other daily life applications. In all the applications, the PCMs are designed to operate at a particular transition temperature with high energy storage density. Although, various solid-liquid phase transition based organic PCM, such as, sugar alcohol, fatty acids and polyethylene glycol, etc. have been significantly investigated for TES due to numerous operating thermal characteristics. Among all, the paraffin wax is the most reliable as a potential PCM due to its

non-toxic nature, large latent heat, no supercooling effect, non-corrosive, operative at the different phase transition temperatures, phase stability, as well as with the possibility for long term usage without degradation[14]. The energy storage in paraffin PCM is a result of van der Waals interaction amongst the long chain polymer molecule[1]. Nevertheless, the low thermal conductivity, flammable nature, and deficiency of control on heat storage duration, heat absorption and heat dissipation temperature, are certain intrinsic limitations[15]. Organic PCM additionally hinder more time for energy storage and release due to the lack of thermal networks which causes the heating source (solar power or waste heat recovery in case of renewable energy & electric power in case of conventional source) to operate for a prolonged duration to charge the PCM, consequently resulting in more energy utilization and therefore confining the TES in large scale applications[16].

A wide spectrum of research has been carried out to enhance the thermal conductivity of paraffin using metal[17], metal oxide[18], metal foams[19] and carbon (single walled carbon nanotube[20], nano fibers[21], multi walled carbon nanotube[22], functionalized multi walled carbon nanotube[23], graphene[24], graphite[25, 26], expanded graphite[27]) nanoparticles and nanostructures, etc. Wang et al.[28] explored the thermal conductivity, thermal stability and cyclability of salt hydrate embedded organic paraffin with expanded graphite as supportive material. Characterization results depict an increase in thermal conductivity of the PCM with 28.9%. Liu et al.[29] conducted experimental investigation on performance of organic PCM with dispersion of graphene nanoplatelets. With 2 wt% graphene nanoparticles the thermal conductivity improved by 21.5% with a drop in energy storage enthalpy by 10.5%. To enhance the phase stability of the PCM, Daou et al.[30] developed a hybrid microencapsulated PCM with paraffin as core material. Metal nanoparticles ZnO, TiO_2 and Fe_2O_3 were opted as a shell material for improving the thermal stability of the synthesized microencapsulated PCM. Inclusion of metal nanoparticles affects the melting enthalpy of the developed composite PCM due to the interfacial interaction. Nevertheless, the drop in melting enthalpy using ZnO nanoparticles is lesser compared to TiO_2 and Fe_2O_3. Wang et al.[31] experimentally evaluated the synergistic effect of porous ZnO and high conductive nature of expanded graphite by dispersing in molten palmitic acid PCM. Maximum increment of 137% in thermal conductivity is due to the adsorbed palmitic acid within ZnO/EG mesopores, thereby developing layered thermal networks, likewise enthalpy reduction of 3% was noticed with 6% of ZnO/EG nanoparticle. Thermal energy storage performance of paraffin with ZnO nanoparticles in tubular shape and powder form was experimentally investigated by Nurten and Paksoy[32]. Latent heat of the ZnO paraffin composite decreased by 7% and 10% for tubular shape and powder form of ZnO

nanoparticles. The inclusion of nanoparticles in PCM results in an increase in thermal conductivity of the PCM. However, these nanostructures contributed to weight gain with increased volume of the composite. Also, the majority of the nanoparticles based PCM composite works resulted in compensation of latent heat of organic PCM with only marginal improvement of thermal conductivity. The role of embedded nanomaterial in PCM composite is very crucial and the selection of appropriate nanomaterial, therefore becomes very important. Nanostructure fulfilling necessary criteria, such as light weight, agglomeration free, electrically and thermally conducting, broad band light absorption, etc. should be carefully explored. The nano-and microstructures from appropriate metal oxide could play a prominent role in this direction[33]. Zinc oxide material from the metal oxide semiconductor family is the most promising candidate to explore its full potential in many different technologies[34]. Nanoparticles of ZnO have been widely used in solar cells, batteries, medicines, cosmetics, and energy storage applications due to their high antibacterial potential, binding energy, UV detection capability and high thermal conductivity[35]. Because of its hexagonal wurtzite crystal structure and robust growth conditions, an extensive range of complex ZnO nanostructural morphologies with the variable surface to volume ratios have been synthesized and utilized in many different technologies[34]. Complex 3D shaped nanostructures from ZnO, e.g., tetrapods and multipods, are very advantageous in the context of composites because they can be easily dispersed without any agglomeration with excellent accessibility of their nanoscopic features. In the milieu of real applications, large scale synthesis of nanostructures via simple methods is very important, which has been successfully demonstrated for ZnO tetrapods growth via reliable flame transport synthesis technique[36, 37]. The tetrapod nanostructures are constructed out of four one dimensional nanorods interconnected via a central core at an angle of around 105° with respect to each other which is directly grown in the single step flame process. The micro and nanoscale ZnO tetrapods exhibit the ability to self-assemble in form of an interconnected well-distributed highly porous entangled networks which offers a lot of advantages in many technological applications. High sensitivity with instant UV response is obtained due to the a) interconnection between tetrapod arms; b) core junction body of the four arms of the tetrapods and c) high porosity of tetrapod nanostructures[38]. On the contrary, the influence of the core junction of tetrapods, the interconnected tetrapod arms, the structure of tetrapod arms are yet to be explored in the area of thermal energy storage, hence the heat transfer mechanism via tetrapods has not been investigated so far to the best of our literature knowledge. The unique properties and 3D shape dependent features motivated us to develop the first tetrapod embedded phase change material (TPCM) composite to explore the potential of ZnO micro and

nano tetrapods for thermal energy storage, harnessing solar radiation and thermal management. PCMs are beneficial in reducing the temperature swings of room spacing and electronic devices, provide provision for thermal energy storage, and also offer long term consistency. Nevertheless to overpower their performance, nanomaterials are dispersed with PCM which tends to reduce the issue of low thermal conductivity. Significant research investigations have been carried out in regard to nanoparticle dispersed PCM to enhance the thermal property and thermal stability of PCM. The profound analysis evidences that the nanoparticles with different dimensions are synthesized and dispersed in PCM for a broad range of applications. The major outspread of 3D nanoparticles discussed with PCM has been so far within the limit of expanded graphite (multiple sheets). Basically the very high surface to volume ratio of the nanoscale structures from various materials exhibit that ability to engineer the properties of PCM for different applications, especially in context to energy. Despite the fact that they can tailor the response of PCM, their appropriate utilization in simple and reliable manner in PCM composites is a challenge. The highly reactive nanoscale surfaces take part in different reactions during handling itself and also they tend to agglomerate which is often undesired. Appropriate selection of the nanostructure, being used as the filler candidate in PCM, thus becomes a very important issue. Apart from the nanoscale surface, the complex shape of nanostructure could play a very important role in this context which has the main focus of present work by utilizing the 3D complex shaped tetrapod nanocrystals from zinc oxide materials as filler candidates in PCM. These 3D shaped zinc oxide tetrapods developed by flame synthesis process have already demonstrated many applications in various directions. The 3D shape offers the unique advantage on the top of functional zinc oxide properties as they do not agglomerate in composites irrespective of how they are handled. Due to their expanding arms in all the three directions, they are able to self-disperse in homogeneously. Inspired by this feature, we aimed to investigate the scope of tetrapod based fillers to engineer different properties of paraffin wax as advanced TPCM composite towards thermal energy storage application.

Herein, for the first time, we report the concept of tetrapod engineered organic PCM composite for potential utilization in harnessing thermal energy by exploring their photonic energy absorption and thermal conductance nature. To date, to evade the problem of low thermal conductivity ample research investigations have been carried out with the dispersion of nanoparticles with PCMs at various concentrations. On a profound observation, it is eminent that nanoparticles with different dimensions are synthesized and dispersed with PCM with stacks of applications. The supreme outspread of 3D nanoparticles discussed with PCM is so

far within the limit of the shape of multiple sheet, nano spheres and hollow tubes. On the contrary, there is extensive research opening in terms of exploring the performance of unique 3D shaped nanoparticles with PCM. In the present work, we expose and outline the exclusive features of tetrapods (unique 3D shaped nanoparticles) towards enhanced thermal energy storage. TPCM of two distinct structures (ZnO tetrapods with thickness of tetrapod arms varying with length of tetrapod arms named as ET nanoparticle; similarly, the other ZnO tetrapod with thickness of tetrapod arms remaining constant throughout the length of tetrapod arms and named as PT nanoparticle) and volume fractions are discretely revealed. We adopted a two-step catalyst free synthesis protocol to prepare a sequence of TPCM composite at different weight concentrations. Compared with base PCM and TPCM composites, the heat transfer properties, optical absorptivity and thermal stability of our fabricated TPCM composites are significantly improved. This is due to the well-developed fine shaped tetrapodal networks, the readily absorbing nature of UV rays and the intermolecular interaction of TPCM. Enthused from the outstanding morphological, chemical, optical and thermal characteristics of TPCM, we further recognize the potential of TPCM towards thermal-thermal energy harvesting and solar-thermal energy transfer performance investigation. In fact, the behaviour of TPCM composite at isothermal conditions during phase transition ensures its high thermal stability and temperature control for better operation without degradation. Inspired by the outstanding thermal-thermal energy harvesting and solar-thermal energy transfer performance of TPCM composite, we further recognize the potential of hybrid tetrapod dispersed PCM for future TES investigation. TPCM composites will be an active candidate for TES in the solar thermal systems and battery thermal management, thereby effectively contributing towards storing clean and affordable energy sources. In addition to that, this research will prove to be very helpful for researchers who want to explore the advantage of 3D structured nanoparticles with extended fins for multi-dimensional energy storage application.

2.0 MATERIALS AND METHODS

2.1 Chemicals: Paraffin RT44HC organic PCM with a phase transition temperature of 44 °C and melting enthalpy of 250 J/g is obtained from RUBITHERM, Germany. Sodium dodecyl benzene sulphonate (SDBS) used as a surfactant, is procured from Sigma-Aldrich, Germany. Zinc powder (diameter of ~ 7.5 µm, 98.8% purity, purchased from Merck, Denmark), Polyvinyl Butyral (PVB) from Kuraray Europe, and ethanol (Sigma Aldrich) were used for ZnO tetrapods growth. 3D ZnO tetrapods of P and E types are synthesized in the laboratory.

2.2 Synthesis of nano 3D tetrapods: ZnO PT & ET nanoparticles were synthesized using flame transport synthesis (FTS)[36] as in Figure S1 A (Supplementary). All chemicals were used without further purification and treatment. For the P-type ZnO tetrapods, a ceramic crucible is filled with a mixture of zinc powder and PVB (as the sacrificial polymer) in a weight ratio of 1:2. The crucible was inserted into a muffle furnace at room temperature, heated at 900 °C for 60 min, then cooled naturally. For the E-type tetrapods, zinc powder is mixed with ethanol in a weight ratio of 2:1 using a magnetic stirrer for 15 min. Then, the solution is brushed at the bottom of a round-bottom ceramic crucible, inserted into a muffle furnace which was pre-heated to 950 °C, and heated at the same temperature for 15 min. In both cases, the obtained white powder is ZnO tetrapods which were carefully harvested and characterized.

2.3 Preparation of TPCM composite: A two-step technique is adopted for preparing the organic TPCM composite dispersed with zinc oxide ET and PT nanoparticle. Figure S1 B (Supplementary) shows the step-by-step procedure for developing the organic TPCM composite with tetrapod nanoparticles at different weight concentrations. 25 g of organic PCM and a required amount of tetrapod nanoparticles (0.5 wt%, 1.0 wt%, 1.5 wt%, 2.0 wt% and 3.0 wt%) was measured by analytical micro balance (EX224, OHAUS). Equal to the weight % of tetrapods, SDBS surfactants were also weighed. Organic PCM were weighed to a quantity so that the total of tetrapod, SDBS and PCM makes 100% for each composition. Measured organic PCM was heated at 70 °C using a hot plate (RCT, BASIC IKA), till the solid phase PCM was transformed into a liquid phase. First weighed nanoparticles are added to the PCM, followed by the inclusion of SDBS to the liquid PCM and sonicated using an ultrasonic bath (EASY 60H, ELMASONIC) for 60 min to ensure uniform dispersion. After sonication, the sample was allowed to cool at room temperature. A similar preparation technique is adopted for preparing all the weight concentrations of both ET & PT nanoparticles. The RT44 paraffin wax is represented as PCM, the other concentration of ET nanoparticle dispersed composite PCM are indicated as PCM/ET-0.5, PCM/ET-1.0, PCM/ET-1.5, PCM/ET-2.0 and PCM/ET-3.0. Likewise concentration of PT nanoparticle dispersed composite PCM are indicated as PCM/PT-0.5, PCM/PT-1.0, PCM/PT-1.5, PCM/PT-2.0 and PCM/PT-3.0.

2.4 Characterization and instruments: Several thermal sensitive instruments were used to examine the morphological, chemical, thermal and light transmission characteristics of the developed TPCM composite. ~~Muffle furnace (Nabertherm GmbH) used for the synthesis of ZnO tetrapods~~. Morphological structures of PCM and the TPCM composite were studied using the instrument Field Emission Scanning Electron Microscopy (FESEM JOEL JSM-7000F

DX). The FESEM instrument was fortified with an Energy Dispersive X-ray Spectroscopy (Oxford Instrument EDX) system, which was operated to determine the elemental compositions of the TPCM composite samples. Fourier transform infrared spectroscopy (FT-IR) (Perkin Elmer, USA) was used to identify the chemical functional group of the tetrapod dispersed PCM samples. The wavenumber range of 400 cm^{-1} to 4000 cm^{-1}, with wave number precision 0.01 cm^{-1} and spectral resolution 0.01 cm^{-1} were chosen to study the chemical composition, as the mid IR spectrum wavelength ranges between 2.5 µm to 25 µm. Optical absorbance and transmittance of the prepared sample in the solar spectrum region were examined using UV-Vis spectroscopy (Model: LAMBDA 750, Perkin Elmer, USA). The readings were taken from a wavelength of 200 nm to 1400 nm at room temperature. UV-Vis spectroscopy of the TPCM composite have been analysed in solid state as the sample exist in solid state at room temperature (20 °C). Thermal properties like thermal conductivity were determined using a thermal property analyzer (TEMPOS), dual needle SH-3, at normal room temperature. A thermogravimetric analyzer (TGA) (Perkin Elmer TGA 4000) is used to conduct a thermal deterioration analysis on pure PCM and the TPCM composite. The temperature for TGA was ramped up to 350 °C at a rate of 10 °C/min in an N_2 environment. The weight and temperature accuracy of the TGA instrument is ±0.02% and 1 °C respectively. Differential scanning calorimetry (DSC) (DSC 3500 Sirius, NETZSCH) was used to analyse the melting temperature and latent heat properties of TPCM composite. DSC melting and cooling curves were inspected between 20 °C and 80 °C under the N_2 atmosphere with a heating rate of 5 °C/min. Thermal cycle tester instrument is used to ensure the thermal stability of the prepared samples. The samples were tested for heating and cooling between the temperatures of 30 °C to 70 °C at 15 °C/min under static environmental conditions. FLIR thermal imaging camera (Cat S60), with thermal sensitivity of 150 mK was used to capture the heating and cooling of TPCM composite samples under solar heating and water bath heating. All curves were plotted in Origin software.

2.5 Solar light to thermal energy conversion: Photo-thermal conversion investigation was carried at indoor conditions, under a solar simulator. A constant input solar radiation of 900 W/m^2 was supplied as an input source. Pyranometer was used to measure solar radiation. The heating was carried out for 4 min, and then the input solar radiation was switched off. Followed by heating the samples were cooled for 16 min. The process of heating and cooling is monitored using a FLIR camera to depict the rise in temperature of the sample. Uniformly for all TPCM composites the temperature was noted from the top centre surface of the sample.

2.6 Thermal to thermal energy conversion: A water bath was maintained at 65 °C, where the 2 g pellets were placed, Figure S2 (Supplementary) represents the methods adopted for preparing the pellets. The heating was carried out for 4 min, after which the samples were removed from the hot bath and allowed to cool for 16 min of cooling at ambient conditions. The process of heating and cooling is monitored using a FLIR camera to depict the rise in temperature of the sample. Uniformly for all samples, the temperature was noted from the top centre surface of the sample. TES using PCM takes place with phase transition from solid to liquid and vice versa. In general PCMs are packed in closed units for energy storage applications. Henceforth in the current experimental evaluation, the PCMs and TPCM composites are placed in a petri dish to avoid loss of PCM in open space application.

3.0 RESULTS AND DISCUSSION

3.1 Morphology and microstructure of tetrapod and TPCM composite

The synthesis of the unique tetrapods, their TPCM composites and corresponding characterizations are elaborated in the experimental section. To understand the mechanism of interaction between tetrapods and PCMs, a direct visual representation of the engineered TPCM composite is presented in Figure 1A, using zinc oxide ET and PT variant nanoparticle (Figure 1B). FESEM image of pure zinc oxide ET & PT nanoparticle are exhibited in Figure 1C and 1E respectively. The FESEM images corresponding to E-TPCM and P-TPCM shown in Figure 1D and 1F clearly reveal the shape integrity and homogenous distribution of tetrapods in the TPCM composite. Even though the shapes are similar, ET & PT nanoparticles differ in terms of the length of arms, the diameter of arms and size of the central core of the tetrapod. Figure 1D indicates the dispersion of ET with each leg designed in a structure of becoming thinner from the centre to the outer edge with PCM at different magnification levels. Figure 1F shows the dispersion of PT with uniform sized arms throughout the centre to the outer edge with PCM. Tetrapod nanoparticles show fin-like extruded arms which are expected to contribute in enhancing the heat transfer rate. In comparison with other 3D nanoparticles such as expanded graphite (stacks of multi-layers)[39]; metal nitride, carbonitride & carbide nanoparticles (spherical shape)[40], the tetrapod with four arms would be unique in terms of shapes with an exceptional surface area which leads to better heat transfer rate due to fin shaped arms. For better visualization the digital images of PCM, TPCM composites, ET & PT are also shown (Figure 1G).

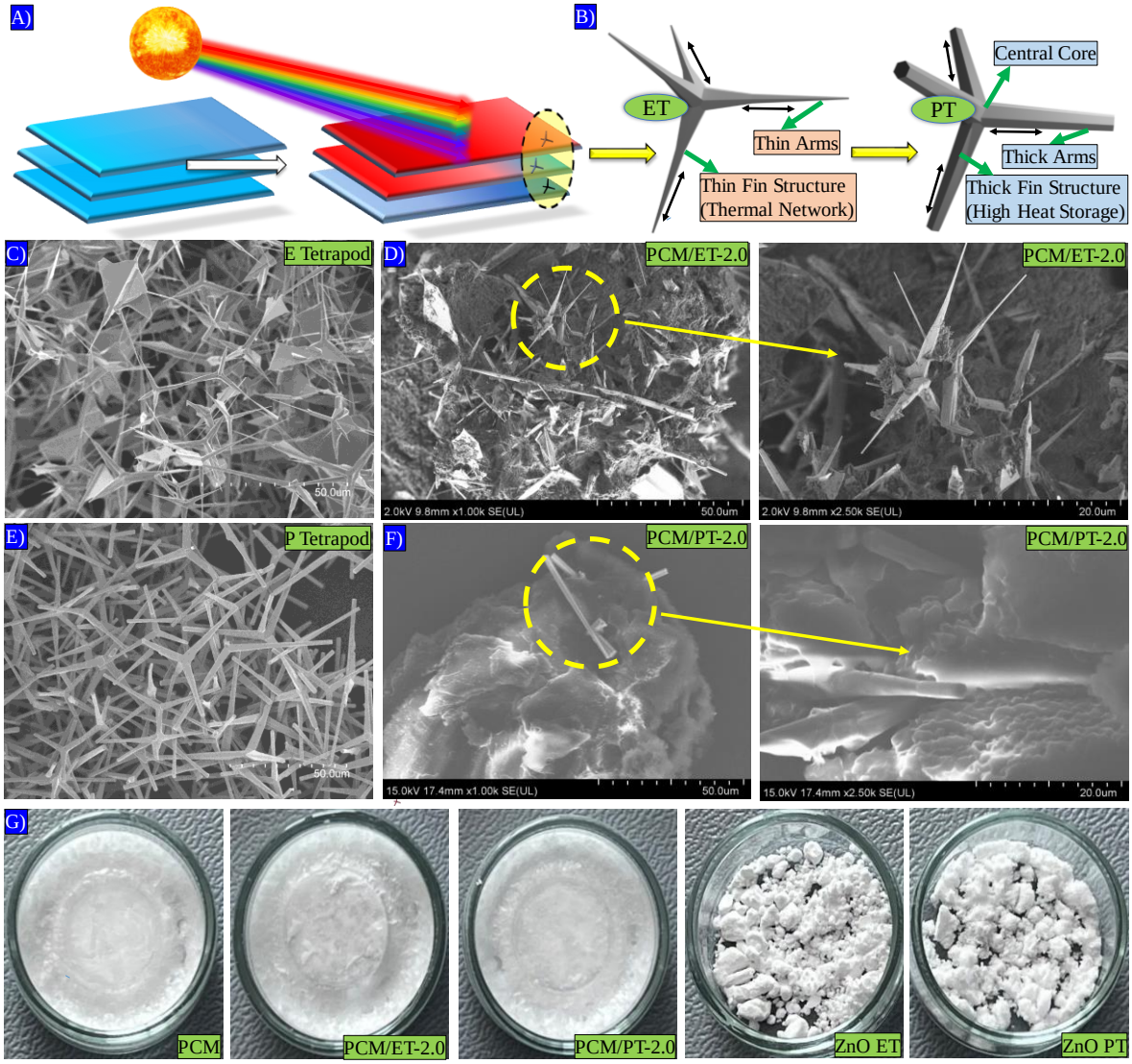

Figure 1*: Behaviour, morphological and microstructure investigation of TPCM composite A) Heat transfer behaviour of engineered TPCM when exposed to solar radiation, B) Structure of ET and PT, ~~Tetrapods with finned arms exhibiting developed thermal network~~ C) FESEM image of E tetrapod, D) FESEM image of ET ~~tetrapod~~ dispersed TPCM composite, ~~at magnification scale of 50 µm & 20 µm.~~ E) FESEM image of P tetrapod, F) FESEM image of PT ~~tetrapod~~ dispersed TPCM composite, ~~at magnification scale of 50 µm & 20 µm.~~ G) Digital image of PCM, ET & PT nanoparticles dispersed TPCM at 2.0 wt% concentration, ET & PT nanoparticle.*

Furthermore, energy dispersive X-ray (EDX) analysis is carried out to understand the micro analysis of the PCM/PT-2.0 and PCM/ET-2.0 composite PCM by elemental mapping and by understanding the electron removed from the inner shells as shown in Figure S3 (Supplementary). The elemental mapping of PCM/PT-2.0 in Figure S3 A (Supplementary)

shows carbon (C) elements to be higher due to their presence in the PCM as paraffin is a long chain polymer with carbon elements. Within the spectrum chosen, C, O, S and Zn elements are identified ensuring the distribution of zinc oxide nanoparticles and SDBS surfactant over the PCM. Similar elements are identified in PCM/ET-2.0 composite PCM in Figure S3 B (Supplementary) along with the wt% of each element in the spectrum chosen for investigation. Figure S3 C (Supplementary) Represent the electron removal in the inner shell such as K, L and M shells when EDX experiment is conducted for the microanalysis. On a whole ZnO tetrapods has a crystal lattice that provides homogeneous dispersion, and the oxygen ratio with Zn is little less than 1:1, these O vacancies takes part in the bonding with neighbouring S (surfactant component) and C (PCM component). Due to the inherent crystal structure of the ZnO, if the distribution is not perfect then there won't be any growth of tetrapods, which is well reported. In addition the 3D shape takes care of the homogenous distribution, as the shape of the tetrapod is a complex shape, hence a perfect distribution cannot be expected and the appear random distribution however they are all the way well connected between them (its the kind of network that is linking between left to right, right to left, top to bottom and bottom to top). They form a sponge-like network which is embedded within the composite.

3.2 Functional group analysis

Understanding the homogenous dispersion and chemical stability of the TPCM composite would support the design of TPCM for further applications based on environmental conditions. The fourier transform infrared (FTIR) spectral analysis is conducted to ensure the chemical interaction between the PCM, tetrapod nanoparticle and surfactant. Paraffin wax is an alkane molecule with the chemical structure C_nH_{2n+2} consisting of straight chained hydrocarbon molecules (n varies from 20 to 40). Figure 2A symbolizes the chemical structure of paraffin molecules belonging to the alkane group. With n number of carbon atoms and 2n+2 number of hydrogen atoms the total number of atoms would be (3n+2). Since every carbon atom in paraffin molecules are sp^3 hybridized they are non-linear, and the number of vibration modes to be exhibited by paraffin with chemical structure C_nH_{2n+2} is (3n-6). Among the (3n-6) vibrations modes of paraffin molecules only 4 modes are IR active, and these peaks are identified at wavenumber 2913 cm^{-1}, 2848 cm^{-1}, 1470 cm^{-1} and 716 cm^{-1} [41]. The spectrum of PCM and its composite with ET nanoparticles are plotted in Figure 2A; similarly, Figure 2B-2C shows the spectrum of PCM with ET & PT nanoparticles. Paraffin PCM with covalent bonds absorbs the selective frequency of infrared radiation (IR) and forms peaks (2913 cm^{-1}, 2848 cm^{-1}, 1470 cm^{-1} and 716 cm^{-1}) in the IR spectral. For a vibrational transition to be IR

active, there must be a change in net dipole moment[42]. The peak at wavenumber 2913 cm^{-1} represents the symmetrical stretching vibration (bond length increases equally) of $–CH_3$, and the peak at wavenumber 2848 cm^{-1} represents the symmetrical stretching vibration of $–CH_2$. Uniform changes in bond length as depicted in Figures 2D and 2E are observed during symmetric vibration of $–CH_3$ and $–CH_2$. The peak at wavelength 1470 cm^{-1} denotes the deformation vibration (change in bond angles) of both $–CH_2$ and $–CH_3$ group[43]. Deformation vibrations occur due to bending modes like wagging, twisting, rocking and scissoring vibrations as illustrated in Figure 2F. The final peak at wavelength 716 cm^{-1} represents the rocking vibration (angular bending of bonds in clock and anti-clockwise direction within the same plane) of $–CH_2$[44].

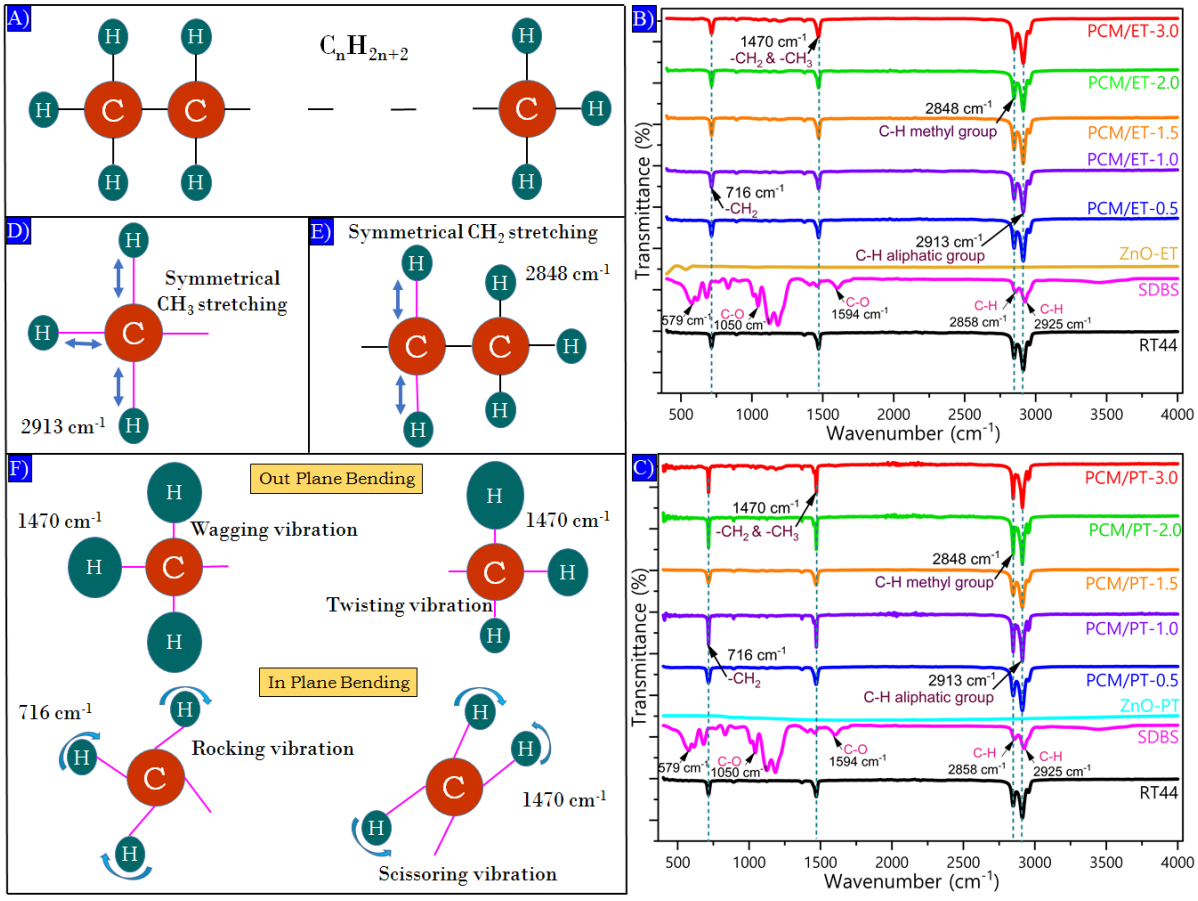

***Figure 2**: FTIR spectral curves of PCM and TPCM composites when observed under FTIR spectroscopy and the bond vibration mechanism behind every peak. A) Structure of paraffin (PCM), with value of n varying from 20 to 40, B) Functional group peaks of PCM, surfactant, ET nanoparticle and their TPCM composite ~~at different wt.%.~~ C) Functional group peaks of PCM, surfactant, PT nanoparticle and their TPCM composite, ~~at different wt.%.~~ D) ~~Representation of~~ Symmetrical CH_3 stretching vibration occurring in TPCM composite at*

wavenumber 2913 cm^{-1} where all the bond lengths are equally stretched, E) ~~Representation of~~ Symmetrical CH_2 stretching vibration occurring in TPCM composite at wavenumber 2858 cm^{-1} where the bond length corresponding to the CH_2 molecules are stretched at equal length, F) Deformation bending vibration between molecules in the same plane (rocking & scissoring vibration) and out plane (wagging and twisting vibration).

No peaks are formed in IR spectral for both ET & PT nanoparticles, thereby ensuring the absence of carboxyl group molecules within the ZnO tetrapod, as well indicates there is no change in net dipole moment. Surfactant sodium dodecyl benzene sulphonate (SDBS) under IR spectral investigation responds both in functional and fingerprint regions. Peaks at 2925 cm^{-1} and 2858 cm^{-1} describe the C-H vibrational mode ensuring the organic group. Peak around 1050 cm^{-1} is due to the energy absorption by C-O groups causing an in-plane vibration. Peaks at the fingerprint region around wavenumber 579 cm^{-1} are a representation of In-O vibration. The presence of acetylacetone is ensured with C-O peak at wavenumber 1594 cm^{-1} [45]. The absence of SDBS peaks in the TPCM composite indicates that surfactant was not adsorbed onto the surface of the base PCM materials, and they have no effect in enhancing the thermal properties of the PCM solely. FTIR spectral analysis confirms consistency among the sample prepared when compared with the original spectral curve of PCM and tetrapod. Absence of new peaks in the TPCM composite sample ensures that interaction between the base and nanoparticle materials is more physical rather than chemical.

3.3 Optical absorption of TPCM composite

Majority of the organic molecules are transparent in the electromagnetic spectrum under the region of 280-720 nm wavelength, accordingly, it is necessary to enhance the absorbance of the organic molecule in the aforementioned region for the enhanced utility of solar energy. Solar radiations being the foremost input energy for TES, the absorptivity of photons by the PCMs are crucial to investigate for effective conversion of light energy into thermal energy. Using a UV-Visible spectrometer the patterns of photo absorptivity of the tetrapod dispersed PCMs are examined. Major concentrations of solar radiation is within the UV rays (7%), visible rays (44%) and near IR rays (37%) spectrum, henceforth the photo absorptivity of TPCM composites are inspected within the range of 280-1400 nm wavelength (280-380 nm UV spectrum; 380-720 nm visible spectrum, 720-1400 nm near IR spectrum)[46]. Discrete absorption behaviour of the PCM, nanoparticles (ET and PT) and surfactant under the aforementioned spectrum are explored and represented in Figure 3(A-C). The absorbance of PCM materials irrespective of the spectrum varies within 0.1-0.18 except for a small broad

peak around 1200 nm. In general, organic PCMs are white in colour and tend to reveal less absorbance than dark materials., However, as the PCM selected belongs to the alkane family, for the absorbance to occur, high energy is required as the electron needs to undergo σ-σ^* orbital transition. A good absorbance value normally ranges between 0.1-1.0, on the contrary the SDBS surfactant material exhibit far below 0.1. On acute analysis, it's noted that the role of SDBS is only to ensure uniform dispersion of nanoparticles within the composite mixture and their sticky nature keeps them dormant to electromagnetic spectrum waves. A noted interesting observation in the behaviour of both tetrapods under the aforementioned spectrum range, under UV region the absorption is high up to 0.8 and forms a wide peak. The maximum absorbance peak for PT (0.8189) and ET (0.7773) occurs at wavelengths of 368 nm and 364 nm, due to high energy intensity at shorter wavelengths of UV spectrum (Figure 3A). Both nanoparticles of ET and PT variant absorb a considerable amount of solar spectrum in the UV-Vis spectrum due to the wide band gap (E_g= 3.37 eV) of the tetrapod and as they ideally detect UV rays[47].

The absorption in ZnO is due to the exciton emission owing to the bandgap 3.37 eV. In addition ZnO has a natural absorption peak in the UV region due to the bandgap. It also has a defect originated absorption into the green band (500-600 nm) depending on the nature of oxygen vacancies. A normal ZnO with defects results in exciton peak and a broad peak. The height of these peaks is interplayed by the defect density and the crystalline nature. In the case of pure ZnO the intensity of the band emission is much higher than green band. Nevertheless, the surface of ZnO is modified on dispersion with PCM molecules. The C element holds the tendency to bond with O element and introduces more of defects resulting in broad absorption spectrum. And when the light penetrates the TPCM samples, the arms of the tetrapods scatter the light rays and the complex scattering process leads to absorption of light rays in a certain wavelength.

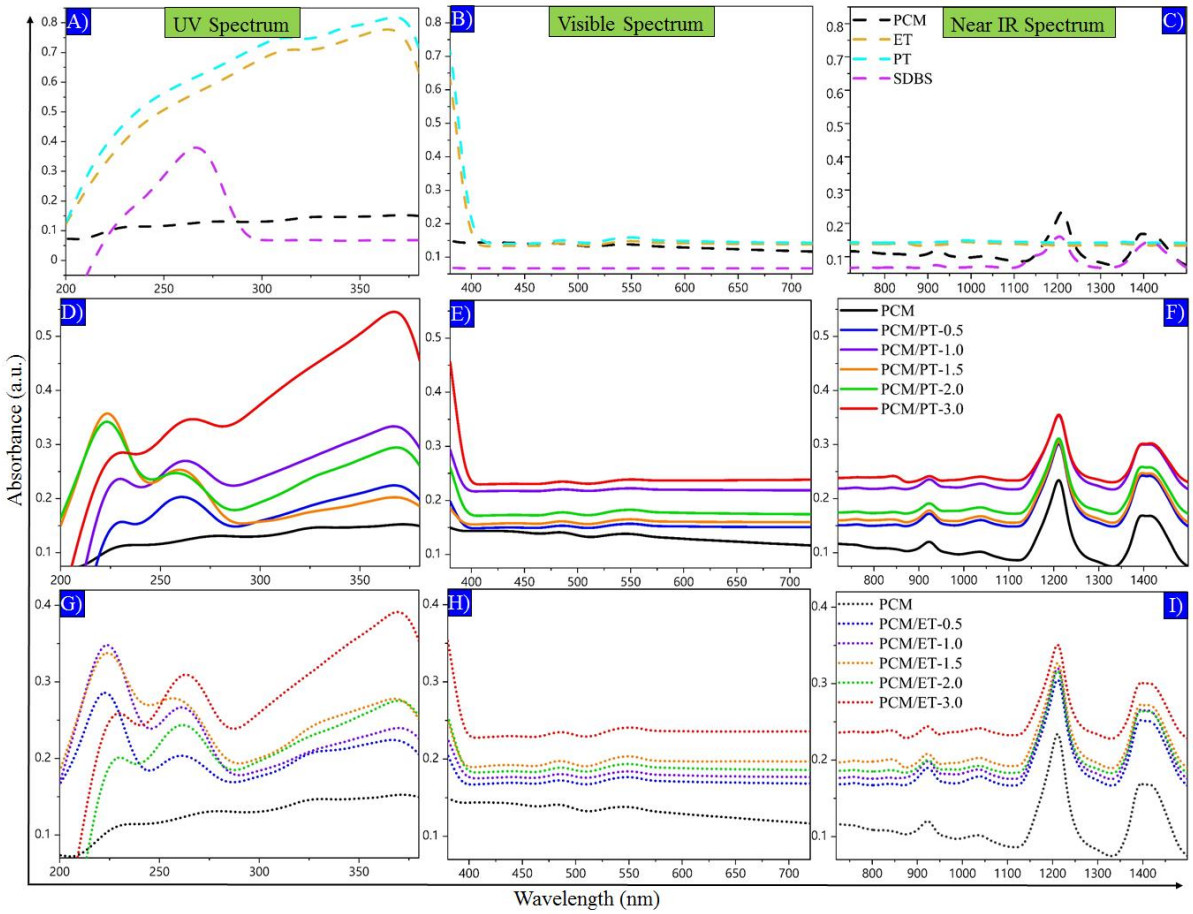

***Figure 3**: Solar spectrum absorbance of PCM, nanoparticles and the TPCM composite when analysed under UV-Vis spectroscopy. ~~A)~~ Photo Absorptivity of base PCM, ET nanoparticle, PT nanoparticle and the surfactant SDBS at A) UV spectrum region (280-380 nm), B) ~~Photo Absorptivity of base PCM, ET nanoparticle, PT nanoparticle and the surfactant SDBS at~~ Visible light spectrum region (380-720 nm), C) ~~Photo Absorptivity of base PCM, ET nanoparticle, PT nanoparticle and the surfactant SDBS at~~ Near IR spectrum region (720-1400 nm); ~~D)~~ Photo Absorptivity of PT nanoparticle dispersed TPCM composite at D) UV spectrum region (280-380 nm), E) ~~Photo Absorptivity of PT nanoparticle dispersed TPCM composite at~~ Visible light spectrum region, (380-720 nm). F) ~~Photo Absorptivity of PT nanoparticle dispersed TPCM composite at~~ Near IR spectrum region (720-1400 nm); Photo Absorptivity of ET nanoparticle dispersed TPCM composite at G) ~~Photo Absorptivity of ET nanoparticle dispersed TPCM composite at~~ UV spectrum region (280-380 nm), ~~H) Photo Absorptivity of ET nanoparticle dispersed TPCM composite at~~ H) Visible light spectrum region (380-720 nm), I) ~~Photo Absorptivity of ET nanoparticle dispersed TPCM composite at~~ Near IR spectrum region (720-1400 nm).*

The absorption behaviour of PT nanoparticle dispersed composite TPCM under the UV, visible and near IR spectrum are signified in Figure 3(D-F). All the prepared composite PCM shows enriched absorbance throughout the spectrum compared to the base PCM. The absorption of PT composites in the UV region reaches a maximum of 0.54 for PCM/PT-3.0 as the higher concentration of tetrapods tends to absorb higher UV rays. Similarly, for PCM/PT-0.5 the maximum absorbance is 0.2 as the concentration of tetrapods is only 0.5%. Likewise, enhanced absorption of the developed TPCM composite in visible and near IR spectral regions ensures the application of TPCM composite for thermal energy storage via photo absorbance. The absorption behaviour of ET nanoparticle dispersed composite PCM under the UV, visible and near IR spectrum are signified in Figure 3(G-I). As inferred from Figure 3(A-C) the absorption of ET nanoparticle dispersed composite PCM is comparatively lower to the absorption of PT nanoparticle dispersed composite PCM. The maximum absorption for PCM/ET-3.0 is 0.39 and for PCM/ET-0.5 is 0.29, the variation in absorption is owing to the lower concentration of tetrapods in the aforementioned TPCM composite samples[48].

On the uninterrupted incidence of radiation over the transparent organic molecule, a share of radiation tends to get absorbed, and with the dispersion of tetrapods, the absorbance is enhanced effectively. When minute energy packets of the solar spectrum strike PCM; photo absorption in a molecule occurs and the electron jumps from the ground level of lower energy to excited level of higher energy. In the UV-Vis spectrometer, the transition in electrons occurs between the various levels of electronic energy, and to be specific for alkanes, the electron transition is between σ-σ^* orbital. The excitation of electrons from σ-bonding to σ^*-bonding is shown in Figure S4 A (Supplementary) when solar spectrum radiation of required energy strikes the element, as well Figure S4 A (Supplementary) illustrates the electronic energy level with increasing energy from the occupied level to the unoccupied level. It is quite obvious that for electron transition in organic molecules to occur higher level of energy is required, which is indeed supplied using solar radiation. However, effective absorbance is possible with uniformly distributed nanoparticles exhibiting better absorbance. In molecules the absorption generally takes place over a wide range of the spectrum, since they exhibit numerous modes of rotations and vibration at ambient conditions. As a result, molecules, have their electrons in many modes of rotational and vibrational excitation. The energy difference for these modes of excitation is less than electronic excitation. Figure S4 B (Supplementary) explains the formation of sigma bonds when two P orbitals overlap in a sideway direction.

3.4 Thermophysical properties and thermal stability

3.4.1 Thermal conductivity

Thermal conductivity of PCMs are a predominant parameter as they highly influence the rate of heat storage/release of thermal energy. We measured the thermal conductivity of the PCM and developed TPCM composites at a room temperature of 25 °C. The composite PCM samples with ET & PT nanoparticles showed an increment in thermal conductivity of 94% and 92% respectively at a concentration of 2.0 wt% as in Figure 4A. Nonlinear increments in the thermal conductivity of the prepared TPCM composite were observed. The thermal performance of PCM with nanoparticles is ascribed due to the formation of thermal networks in both vertical and horizontal directions especially at the low filler spots[49]. Furthermore, the tetrapod initiates thermal energy transfer carrier movement at the tips. In addition, the tetrapod exhibits a higher surface to volume ratio, consequential leading to enhancing the mobility of tetrapod nanoparticles and accelerating the phonon interaction for heat transfer[44]. The arm structures of tetrapods act like a fin to connect strong thermal pathways. Besides, all the inclusion of nanoparticles with higher thermal conductivity compared to the base material contributes to enhancing the thermal conductance. With an increase in the concentration of tetrapod the thermal conductivity of PT nanoparticles are dominant due to their microstructure compared to the nanometric structure of ET nanoparticles until 1.0 wt% concentration. At higher concentration above 1.0 wt% as PT nanoparticles are thicker, find it difficult to channelize proper conducting paths, whereas ET nanoparticles being thinner and due to a higher aspect ratio (surface area to volume) tends to develop better thermal networks and increases thermal conductivity. With higher concentration, both ET and PT nanoparticle agglomerate and tend to form clusters and show settling their results in a drop of thermal conductivity. Thermal conductance of the TPCM composite is of utmost concern as it results in effective charging and discharging of thermal energy.Thus, TPCM composite with 2.0 wt% of PT & ET nanoparticles are opted to be the best suited combination and their thermal cycling nature, thermal conductance and photo absorbance in real time application are further investigated and compared with base PCM.

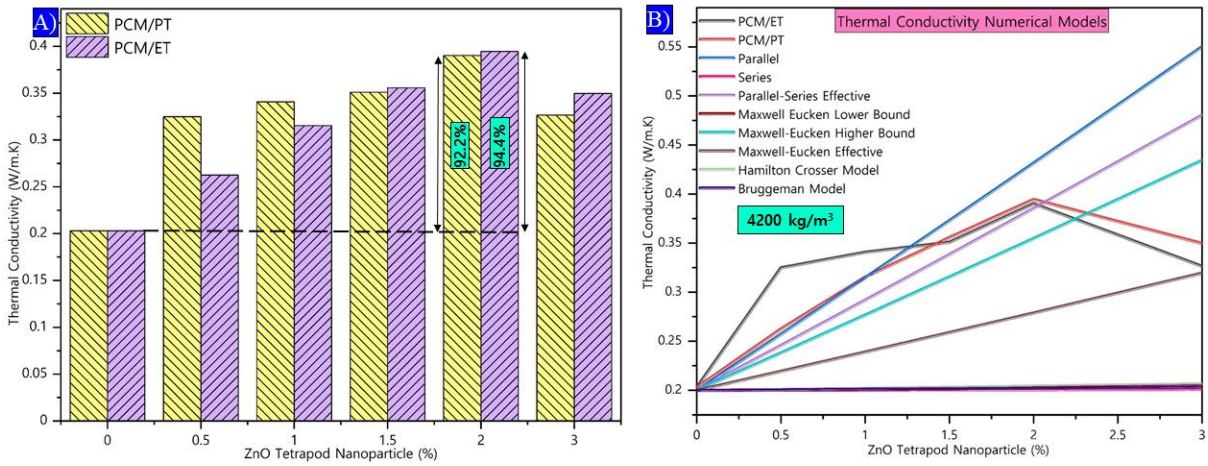

Figure 4: ~~*Thermal conductivity of PCM ensuring the rate of heat storage and release for effective TES.*~~ *A) Thermal conductivity of composite PCM with dispersion of ET & PT nanoparticles. B) Comparison of experimental thermal conductivity of TPCM composite with numerical models.* ~~*used to determine thermal conductivity of fillers dispersed polymeric composites.*~~

The thermal conductivity of the polymeric composites are highly variable by the thermal conductive fillers (nanoparticle), and interfacial thermal resistance between the fillers and polymer composites. Micro and nanostructure of the composite, fraction of filler, shape of the nanoparticle and uniform distribution are a few added parameters that impacts the thermal conductivity of the composites prepared[50]. The experimentally obtained thermal conductivity values of the TPCM samples are compared to thermal conductivity values calculated based on the numerical models viz. parallel model, series model, Maxwell Eucken model, Hamilton model and Bruggeman model[51] as plotted in Figure 4B. The thermal conductivity equations used in parallel model, series model, Maxwell Eucken model, Hamilton model and Bruggeman model are listed in Equation E1-E5 (Supplementary). Each model describes a unique arrangement of nanoparticles with polymer composites. To begin with parallel model, nanoparticle dispersed with base PCM tends to arrange themselves in an analogous manner and ensures uniform distribution of nanoparticle to effective transfer heat flux. On the contrary in series model, the nanoparticle and the polymeric composite arrange in a succession connection and the nanoparticle agglomerates and results in settling down. As an outcome of the series arrangement, the thermal conductivity of the polymeric composite is less and results in a low heat transfer rate. Both parallel and series models of nanoparticle arrangement are extracted from the Fourier heat conduction technique. The parallel and series models are a combination of parallel and series arrangements of nanoparticles, where the thermal conductivity and heat

flux rate are comparatively better than the series model. In addition, the Maxwell Eucken model potentially extracts the thermal conductivity where nanoparticles of uniform sphere shapes don't tend to interact between corresponding nanoparticles and forms a random dispersion in polymeric composite. Furthermore, the Hamilton crosser model considers the shape of nanoparticles in terms of sphericity, in the present numerical evaluation, the sphericity of tetrapods are assumed to be 0.53, and the calculated thermal conductivity is very low and it indicates non uniform distribution of nanoparticle. In conclusion, the thermal conductivity models discussed are the Bruggeman model, which is effective for two phase polymeric composite, (i.e. dispersion of nanoparticles up to 30% with the base material). Since the higher fraction of tetrapod preferred in the current research is 3.0 wt%, the Bruggeman model results aren't preferred to determine the thermal conductivity. Based on the evaluated models, the parallel model is the highly preferable model for determining the thermal conductivity of tetrapod dispersed polymeric phase change materials for better supporting evaluation.

3.4.2 Latent Heat

Latent heat of PCM ensures the energy density and the limit of TES during phase transition. Foremost parameter to confirm the suitability of PCM to store energy depends on phase change enthalpy. Higher the phase transition enthalpy of the material higher is the energy storage; similarly, enthalpy efficiency in terms of discharging the energy stored during the charging process is highly significant. Figure 5A and 5B portrays the state of PCM during the heating and cooling process. Latent heat curves during the heating and freezing of TPCM composites at different weight concentration are recorded using differential scanning calorimetry (DSC) as represented in Figure 5D and 5E. The variation in latent heat value is compared in Figure 5C, which indicates a 3% improvement for TPCM compared to the base PCM. The endothermic peaks in the melting curve are a result of heat storage or heat enthalpy of the TPCM composite, likewise, the exothermic peaks represent the heat released during the phase transition from liquid to solid. Two peaks are observed during exothermic peaks, where the broad peak represents the liquid-solid phase transition of PCM, and the sharp peak around 33 °C represents the solid-solid phase transition which is common in high concentrated PCMs. The phase change temperature of all the TPCM composites are non-predictive and varies non-linearly based on the concentration of the nanoparticle. Furthermore, in distinct to extensively stated composites, where the dispersion of nanoparticles with PCM tends to considerably reduces the latent heat value and heat storage capability, nevertheless, we report an increase in the latent heat value of TPCM composites. Melting enthalpy of pure PCM is determined to be

239.8 J/g, whereas for PCM/PT-1.0 the latent heat value is 248.3 J/g which shows a 3.5% increment. The latent heat of TPCM composite with PT nanoparticle tends to increase till a concentration of 1.0 wt% and tends to drop further for any concentration above 1.0 wt% tetrapods, however until 3.0 wt% concentration of tetrapods the latent heat of the TPCM composite were equal to the base PCM. Superior thermal energy storage potential of TPCM composite is attributed due to the porosity nature of ZnO materials of tetrapods[52], which improves the intermolecular force of attraction between the tetrapod and PCM as the PCM have meshed with the pore of tetrapod void[53]. In addition, latent heat is the energy required to modify the crystalline structure of material from solid to liquid phase, as well the thicker arms of tetrapods contribute to effectively uphold the energy supplied. In regard to PCM/ET-2.0, a slight drop of less than 1% in latent heat value is noticed, which can be ascribed due to the thin arms of tetrapods, where the energy storage potential is slightly lower than PCM/PT-2.0. A further significant point to observe is the degree of supercooling, from Figure 5D and 5E it can be inferred that all the TPCM composite and base PCM have a common temperature at which the melting and freezing initiates, which ensures zero degree of supercooling. This is highly observed in inorganic salt hydrate PCMs due to the mixture of salt and hydrate molecules at different phases.

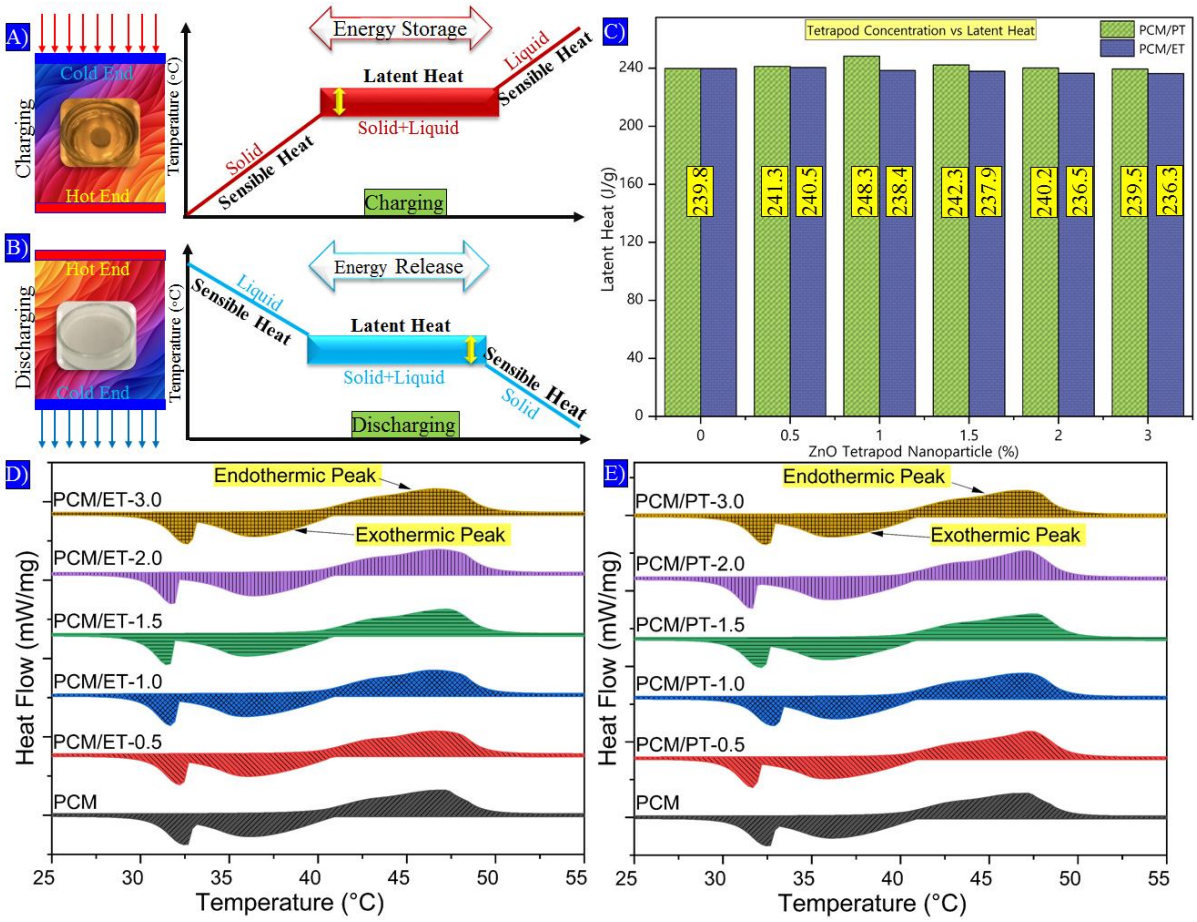

Figure 5*: Melting enthalpy of tetrapod dispersed PCM for effective TES. A) ~~When heat energy is supplied, PCM stores thermal~~ Energy storage in PCM during phase transition from solid to liquid, ~~maximum energy storage in phase change material occurs in the form of latent heat, this process is generally termed as charging.~~ B)Energy release from PCM during phase transition liquid to solid, ~~During the discharging process the PCM starts cooling, thereby releasing the stored thermal energy and regains its solid phase from liquid phase with drop in temperature. PCM exhibits equal amounts of heating and cooling enthalpy during phase transition.~~ C) Comparison of enthalpy value for ET & PT nanoparticles dispersed TPCM composites at different concentrations, D) Endothermic peaks of ET nanoparticles dispersed TPCM composites at different concentrations, E) Endothermic peaks of PT nanoparticles dispersed TPCM composites at different concentrations.*

3.4.3 Thermal Decomposition Analysis

Thermal decomposition curves for PCM and TPCM composites at various concentrations are plotted in Figure 6A and 6B to evaluate their thermal stability, maximum decomposition point and the decomposition kinetics of the materials. The samples tested show a single step thermal degradation within the temperature of 25 °C to 380 °C. Normally, the

582 decrease in weight percentage of the sample in a thermogravimetric analyzer (TGA) is due to
583 evaporation, decomposition, desorption and reduction. Weight loss in base PCM is attributed
584 owing to the breakdown of long chain polymeric material into monomers when heated at higher
585 temperatures and decomposition occurs between 155 °C (point up to which PCM and tetrapods
586 are dispersed and available for heat storage as indicated in Figure 6A and 6B) and 277 °C (point
587 at which only the residues of tetrapod nanoparticle are seen as the PCM gets completely
588 degraded as shown in Figure 6A and 6B). The maximum weight loss occurred for the best
589 opted (based on thermal conductivity) TPCM composite PCM/ET-2.0, PCM/PT-2.0 and base
590 PCM were 92.5%, 95.25% and 99.2% as in Figure 6C. It can be inferred that for PCM/ET-2.0
591 the residue is only 4.8% (weight loss of 95.2%) whereas for PCM/PT-2.0 the residue is 7.5%
592 (weight loss of 92.5%). This is ascribed due to the unique structure of E tetrapods, which
593 exhibit a thin arms and undergoes better decomposition than P tetrapods with thick arms. All
594 ET nanoparticle dispersed PCM samples tend to lose weight by initializing decomposition at a
595 temperature of 155.6 °C (as in Figure 6A). And the maximum decomposition point for ET
596 nanoparticle dispersed PCM samples PCM/ET-0.5, PCM/ET-1.0, PCM/ET-1.5, PCM/ET-2.0
597 and PCM/ET-3.0 are around 289 °C, 283.5 °C, 282 °C, 278 °C and 275.5 °C respectively.
598 Similarly, all PT nanoparticle dispersed PCM samples tend to lose weight by initializing
599 decomposition at a temperature of 161 °C (as in Figure 6B). And the maximum decomposition
600 point for PT nanoparticle dispersed PCM samples PCM/PT-0.5, PCM/PT-1.0, PCM/PT-1.5,
601 PCM/PT-2.0 and PCM/PT-3.0 are around 274 °C, 290 °C, 280 °C, 286 °C and 282 °C
602 respectively. Inclusion of tetrapod nanoparticles assisted thermal resistance with an increase in
603 temperature and improved the decomposition temperature of the polymeric TPCM composite
604 samples and delayed the decomposition compared to the base PCM, which is endorsed due to
605 the potential of tetrapods to absorb the heat supply, and provided thermal resistance for
606 extended range of temperature[32].

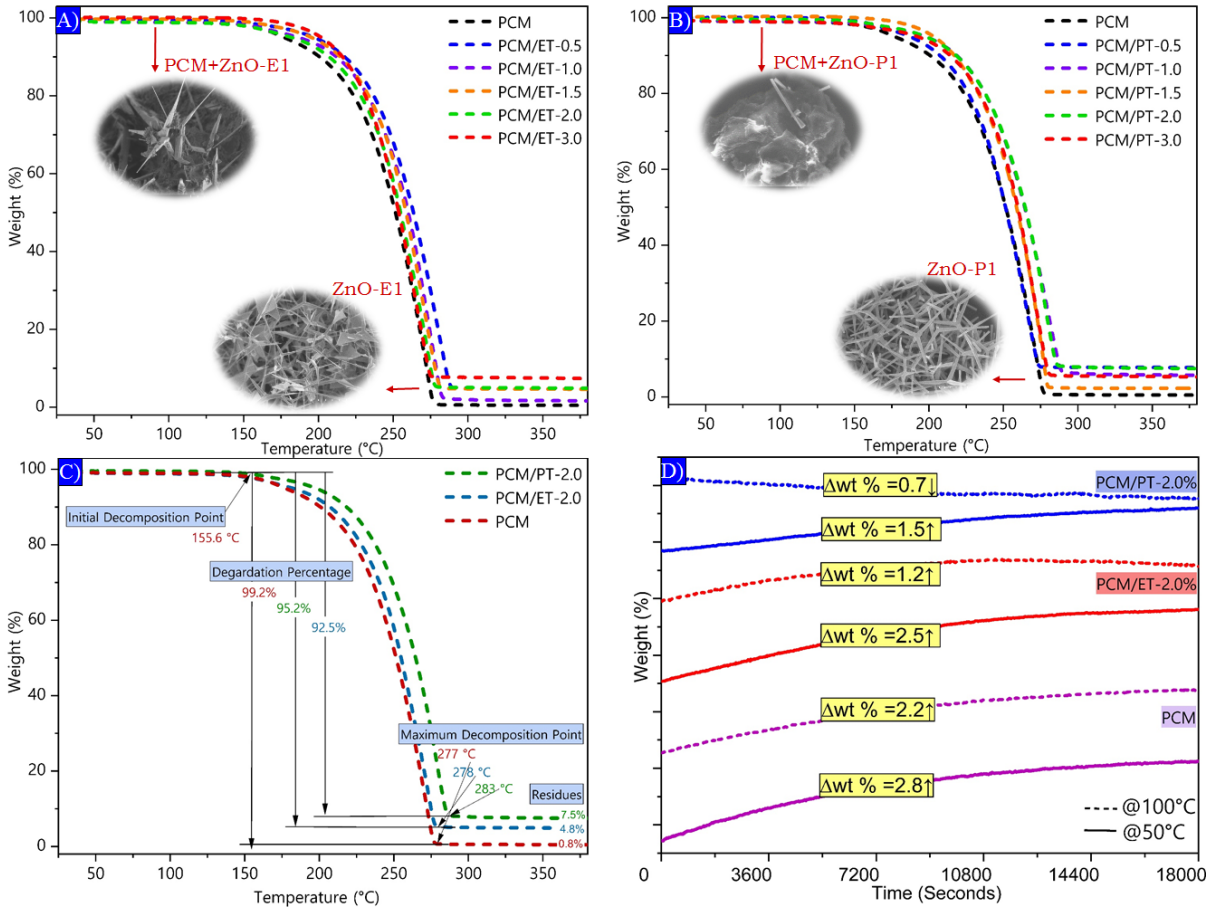

***Figure 6**: Thermo gravimetric analyser curve of ET & PT nanoparticles dispersed TPCM composite ensuring the thermal decomposition point. A) Thermal decomposition temperature analysis of ET nanoparticle dispersed TPCM composite, ~~at different concentrations. Both PCM and E tetrapod nanoparticles are well distributed till 155.6 °C, from there on the PCM starts decomposition and around temperature 278 °C residues of E tetrapods are available as nanoparticles have high melting and degradation points.~~ B) Thermal decomposition temperature analysis of PT nanoparticles dispersed TPCM composite, ~~at different concentrations.~~ C) Thermal decomposition temperature analysis of PCM, PCM/ET-2.0 & PCM/PT-2.0 nanoparticle dispersed TPCM composite sample, D) Isothermal investigation of the PCM, PCM/ET-2.0 & PCM/PT-2.0 ~~nanoparticle dispersed TPCM~~ composite sample at 50 °C and 100 °C for five hours.*

The phase transition and the energy release and storage of PCM are completely driven by external environmental conditions, in the case of medium temperature application. When the atmospheric temperature goes high compared to the transition temperature of PCM, energy is absorbed by PCM, and vice versa when the atmospheric temperature drops below the transition temperature of PCM. In consequence, it is important to understand the changes

occurring in a PCM sample when they are treated at an isothermal (constant temperature) state. Isothermal evaluations of the sample are analysed to understand the decomposition percentage of PCM samples when they are allowed to be at a constant temperature for a longer duration. Furthermore, PCM, PCM/ET-2.0 and PCM/PT-2.0 composites are evaluated at isothermal conditions of 50 °C (just above phase transition temperature) and 100 °C (as aforementioned maximum temperature of waste heat from industries are at this range) for duration of 5 h; to evaluate the weight loss in PCM as shown in Figure 6D using TGA instrument. Since the decomposition temperature of the composite samples prepared is 155 °C, the isothermal nature is evaluated at two different temperatures prior to the decomposition point. Interestingly we notice increased trends in weight fraction of the TPCM composite samples with base PCM leading the PCM/ET-2.0 & PCM/PT-2.0 respectively at both 50 °C and 100 °C. In increase in weight % of the sample during isothermal condition are mostly attributed due to adsorption, desorption and oxidation. However, on keen analysis, it's been noted that the purity of the N_2 gas used for heating is high and doesn't cause deposition of any particles from air on to the surface of sample.Similarly, oxidation in alkane samples is not likely to occur, as they release heat with the formation of carbon dioxide and water. The most probable possibility is that the density of gas around the sample crucible tends to get less dense with temperature and the pan is likely to experience a lower buoyant lift and tends to cause an increase in weight. Nevertheless, the weight changes are very minimal within the range of -0.7% to 2.5% for the tetrapod dispersed samples.

With application focus, PCM with phase transition temperature in the range of 44 °C to 47 °C have been very attractive for photovoltaic thermal (PVT) systems, battery thermal management and electronic cooling applications where the ZnO tetrapod dispersed PCM would work efficiently without any decomposition.

3.4.4 Thermal cycling study

Thermal stability of the tetrapod nanoparticle dispersed polymeric TPCM composites are investigated using a thermal cycler to confirm long term resilience of the PCM. Base PCM and TPCM composites with 2.0 wt% were examined after 300 and 600 thermal cycles. During thermal cycling evaluation, the samples were heated to a maximum of 80 °C and cooled to a temperature of 25 °C. Chemical and thermal characteristics of TPCM with 2.0 wt% after 300 thermal cycles and 600 thermal cycles are depicted in Figure 7 (A-C). The chemical stability of the TPCM composites are characterized using FTIR after repeated number of phase transfer. Alkane vibration stretching has been observed (2913 cm^{-1}, 2848 cm^{-1}, 1470 cm^{-1} and 716 cm^{-}

[1]) for base PCM and TPCM composites after 300 and 600 thermal cycles as can be observed in Figure 7A, ensuring their chemical stability. Photographic views of TPCM composite are shown in Figure S5 (Supplementary) to have a better understanding of the physical appearance of PCM and TPCM composites after repeated thermal cycles.

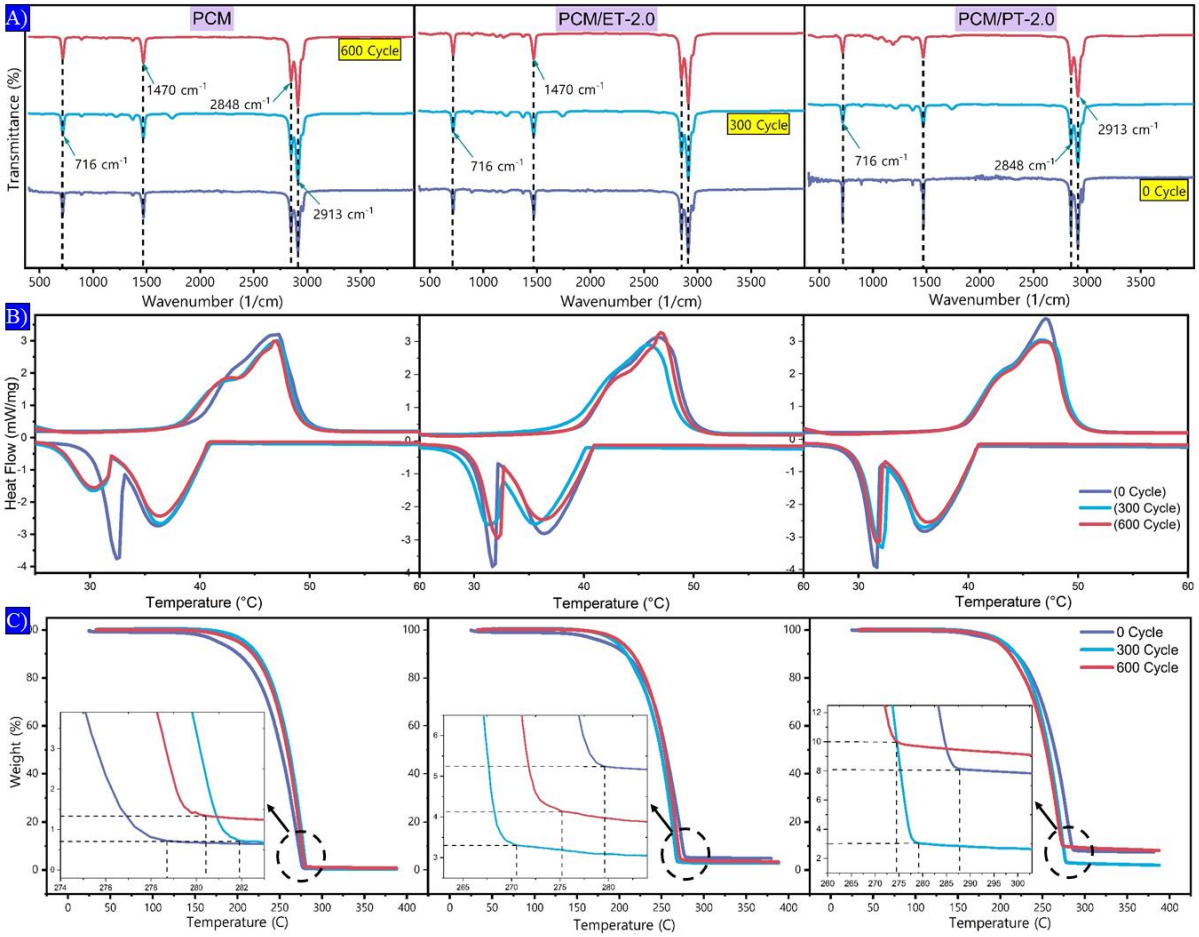

***Figure 7**: Thermal stability analysis of TPCM composites for 600 heating and cooling cycles. A) Evaluation of ~~a functional group using~~ FTIR spectrum for base PCM, PCM/ET-2.0 and PCM/PT-2.0 after 0, 300 and 600 thermal cycles, B) Endothermic and exothermic peak comparison of PCM, PCM/ET-2.0 and PCM/PT-2.0 after 0, 300 and 600 thermal cycles, C) TGA analysis of base PCM, PCM/ET-2.0 and PCM/PT-2.0 after 0, 300 and 600 thermal cycles.*

Followed by chemical stability, the thermal stability of the samples are ensured using DSC and TGA instruments to understand the change in latent heat and the decomposition point. We determine the latent heat value and the melting point of TPCM composite PCM after 300 & 600 thermal cycles using heating curves obtained from the DSC instrument (Figure 7B). Latent heat of PCM, PCM/ET-2.0 and PCM/PT-2.0 after 600 thermal cycles were 218.9 J/g, 225.4 J/g & 226.4 J/g. By evaluation its evident that latent heat of PCM drops by 8.72%, PCM/ET-2.0 drops by 4.7%, and PCM/PT-2.0 drops by 5.74% which shows a notable less drop

in enthalpy compared to the base PCM thereby confirms the potential of TPCM composites for real time application. Further, the DSC plots also indicate the stability of PCM for long term heating and cooling cycles. The thermal stability of the composite material and the weight fraction of residue particles with an increase in temperature of the samples are evaluated for 0, 300 and 600 thermal cycles using TGA (Figure 7C). Weight fractions of the TPCM composite sample after 300 and 600 period of thermal cycles were approximately similar to the sample without any period of thermal cycle until a steep drop occurs at a temperature range of 170–280 °C, above which the residue materials are present.

However, the authors would like to comment on the stability of the nanoparticle (ZnO Tetrapods), followed by the stability of the TPCM composite. The ZnO tetrapods are physically very robust; mechanically they are very stable up to 400 °C temperature. In general over the number of thermal cycles there might be little re-adjustment in the composite, due to the phase transition between solid to liquid and liquid to solid, which is problematic and common in standard nanoparticle systems due to agglomeration. Nevertheless, with the unique tetrapods, the 3D shape holds the advantage as there could be very little adjustment and the 3D arms will ensure uniform dispersion, this re-adjustment will occur only in the few initial cycle, and the dispersion of network is going to be homogenous irrespective of the number of cycles as it only undergoes phase transition from solid to liquid and liquid to solid. In addition no mechanical stress is applied during the phase transition. Thermal stability of the TPCMs are a critical pointer to evaluating their energy storage regulation during practical use. The FTIR spectral curves (Figure 7A), DSC heating and cooling curve (Figure 7B) and thermal degradation curve (Figure 7C) of TPCMs are recorded after repeated thermal cycles. It can be ensured from the FTIR spectral curve that no new peaks or significant changes are observed in the pattern after repeated thermal cycles, which ensures the chemical stable nature of TPCMs. Minimal drop in heating and cooling enthalpy value was obtained, but significantly better than the base PCM. Similarly, the thermal degradation curve of TPCM shows early degradation by 2-3 °C, but is comparatively better than base PCM. The intermolecular interaction and better conducting nature of the tetrapods ensure superior thermal stability for the TPCM reported even after repeated thermal cycles.

3.5 Evaluation of TPCM composite for thermal conductance and photo absorbance

Energy storage within PCMs is attained by an input supply of either light energy or heat energy. In consequence, it is very important to access the real time performance of TPCM. An experimental investigation has been carried out on the solar driven and heat driven TPCM

composites to understand better the light-thermal conversion performance and heat-thermal conversion performance of the optimum samples (PCM/PT-2.0 & PCM/ET-2.0).

3.5.1 Photo-thermal conversion

With solar energy being the most abundant and easily used renewable energy source, the conversion of photons from solar rays into thermal energy are remarkable characteristic. Here, the behaviour of tetrapods in enhancing the thermal energy storage of PCMs is analysed. Temperature distribution of the TPCM composites during heating and cooling process are visualized using IR camera and the change in temperature is digitally represented in Figure 8 (A-B). 2 g pellets of base PCM, PCM/PT-2.0 and PCM/ET-2.0 are taken for the experimental investigation as in Figure S6 (Supplementary). Temperature distribution during the heating and cooling process of the TPCM composites is plotted in Figure 8C. During the heating process the absorbance of solar radiation by the PT nanoparticle composite is more influencing than, ET nanoparticle composites and the base PCM. Temperature difference between base PCM and PCM/PT-2.0 is 6.3 °C. The rise in temperature of the PT nanoparticles is well understood by the absorbance characteristic of the PT nanoparticle and their TPCM composite compared to the ET nanoparticles. Absorptivity of PCM/PT-2.0 and PCM/ET-2.0 samples are improved compared to the base PCM, as the ZnO tetrapods effectively detect UV rays and tend to exhibit the same behaviour on uniform distribution over the base PCM.

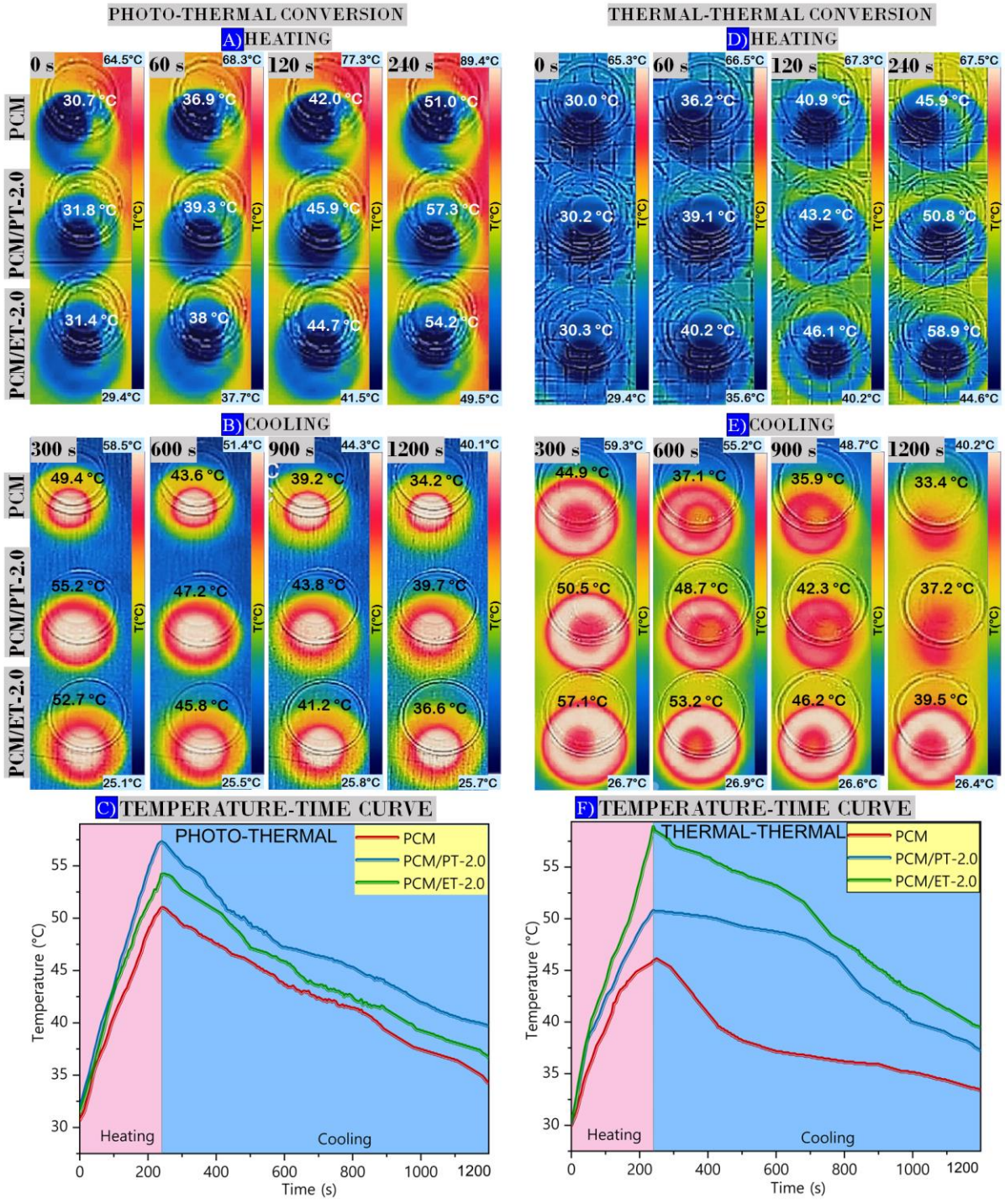

725

726 ***Figure 8***: *Photo-Thermal energy conversion evaluation of the prepared TPCM composite*
727 *using solar simulator. A) Temperature distribution of base PCM, PCM/ET-2.0 and PCM/PT-*
728 *2.0 during heating for 4 min. B) Temperature distribution of base PCM, PCM/ET-2.0 and*
729 *PCM/PT-2.0 during cooling for 12 min, C) Temperature time curve for heating and cooling of*
730 *base PCM, PCM/ET-2.0 and PCM/PT-2.0 during the photo-thermal energy conversion;*
731 *Thermal-Thermal energy conversion evaluation of the prepared TPCM composite using water*
732 *bath maintained at 65 °C. D) Temperature distribution of base PCM, PCM/ET-2.0 and*

PCM/PT-2.0 during heating for 4 min, E) Temperature distribution of base PCM, PCM/ET-2.0 and PCM/PT-2.0 during cooling with temperature drop for 12 min, F) Temperature time curve for heating and cooling of base PCM, PCM/ET-2.0 and PCM/PT-2.0 during the photo-thermal energy conversion.

~~*Figure 8: Photo-Thermal energy conversion evaluation of the prepared TPCM composite. A) Temperature distribution of base PCM, PCM/ET-2.0 and PCM/PT-2.0 during heating using a solar simulator for 4 min. B) Temperature distribution of base PCM, PCM/ET-2.0 and PCM/PT-2.0 during cooling with temperature drop for 12 min. C) Experimental setup used for evaluation of light to thermal energy conversion using solar simulator. D) Capture of thermal image plots using FLIR thermal imaging camera. E) Temperature time curve for heating and cooling of base PCM, PCM/ET-2.0 and PCM/PT-2.0 during the photo-thermal energy conversion experimentation.*~~

3.5.2 Thermal-thermal conversion

In addition to photo-thermal conversion evaluation, a thermal-thermal conversion is also experimentally investigated as represented in Figure S7 (Supplementary). Temperature distribution of the TPCM composite samples are visualized using an IR camera and the change in temperature is digitally represented in Figure 8 (D-E). Similar to the samples used in photo-thermal conversion investigation, for uniformity 2 g of base PCM, PCM/PT-2.0 and PCM/ET-2.0 composites are preferred. Temperature distribution during the heating and cooling process of the samples is plotted in Figure 8F. During the heating process, all the samples tend to respond similarly in the initial few seconds, nevertheless as the pellets start melting and as the heat penetrates the TPCM composites, the ET based TPCM composites are more dominant than others in conducting thermal energy and reach a maximum of 58.9 °C within 4 min. This phenomenon predominantly indicates the thermal network paths formed by ET nanoparticles for effective thermal energy transfer. PT nanoparticles are also inspiring compared to the base PCM, the PT nanoparticles due to their size face issues with creating proper thermal networks for heat transfer and reach a maximum of 50.8 °C during the heating process. However, it's interesting to notice better heat storage and slow heat dissipation rate in PT nanoparticles, during cooling, whereas the ET nanoparticles exhibit a fast heat dissipation rate due to the well-formed thermal path networks.

The most important phenomena to observe are the method of heat supply during the photo-thermal energy conversion experiment and heat-thermal energy conversion experiment, and the point from which the temperature is measured. During photo-thermal energy conversion, the input radiation strikes the top surface of the sample and slowly transmits the

energy to the bottom, as there is no energy transfer due to the movement of molecules, and it's only due to the collision of molecules. This results in a high surface temperature of the sample during the emission of solar radiation. On the other hand, during a heat-thermal energy conversion experiment, the heat input is supplied from the bottom, and the pellets transmit heat from the bottom surface to the top, the heat transmission phenomena occurs by the movement of molecules. It is clear from the experiment conducted that, heat-thermal energy conversion are very effective in TPCM which is supported by the thermal conductivity value obtained, and photo-thermal energy conversion occurs based on the absorbance characteristic of the sample which is well justified with the UV-Vis spectroscopy analysis.

~~*Figure 9: Thermal-Thermal energy conversion evaluation of the prepared TPCM composite. A) Temperature distribution of base PCM, PCM/ET-2.0 and PCM/PT-2.0 during heating using a water bath maintained at 65°C for 4 min. B) Temperature distribution of base PCM, PCM/ET-2.0 and PCM/PT-2.0 during cooling with temperature drop for 12 min. C) PCM and TPCM composites chosen in pellet form for experimental investigation. D) Experimental setup arrangement during heating of samples using hot water bath to evaluate thermal to thermal energy conversion. E) Experimental setup arrangement during cooling of samples at ambient condition. F) Temperature time curve for heating and cooling of base PCM, PCM/ET-2.0 and PCM/PT-2.0 during the thermal-thermal energy conversion experimentation.*~~

4.0 CONCLUSION

In summary, we present the developed organic solid-liquid TPCM composite with a unique featured tetrapod for solar heat energy storage systems. Among the TPCM composite, we advanced with highly efficient thermal energy charging rate and photonic energy harnessing characteristics with improved solar spectrum absorbance. The TPCM composites achieved 92-94% of enhancement in thermal conductance and an 11% increment in photo absorbance of the solar spectrum. There is no compensation in latent heat of TPCM composite; chemical and thermal stability is ensured after repeated thermal cycles of operation, which makes the developed TPCM composite attractive and reliable for numerous energy storage applications. Developed TPCM composite unwraps new systems for effective low cost solar energy based TES systems like distillation unit, photovoltaic thermal system and waste heat recovery units.

ACKNOWLEDGEMENT

One of the author (Adarsh Kumar Pandey) acknowledges the financial assistance of Sunway University through Sunway University's Internal Grant Scheme (GRTIN-IGS-RCNMET[S]-

15-2022) for carrying out this research. Author (Yogendra Kumar Mishra) acknowledges the fundings by Interreg Deutschland–Denmark with money from the European Regional Development Fund, project number 096-1.1-18 (Access and Acceleration), BHJ Fonden Denmark, and Fabrikant Mads Clausen Fond, Denmark.

REFERENCE

1. M. A. Gerkman and G. G. Han, *Joule*, 2020, **4**, 1621-1625.
2. P. Albertus, J. S. Manser and S. Litzelman, *Joule*, 2020, **4**, 21-32.
3. S. Koohi-Fayegh and M. A. Rosen, *Journal of Energy Storage*, 2020, **27**, 101047.
4. V. Kashyap, S. Sakunkaewkasem, P. Jafari, M. Nazari, B. Eslami, S. Nazifi, P. Irajizad, M. D. Marquez, T. R. Lee and H. Ghasemi, *Joule*, 2019, **3**, 3100-3111.
5. T. Yang, W. P. King and N. Miljkovic, *Cell Reports Physical Science*, 2021, **2**, 100540.
6. B. Kalidasan, A. Pandey, R. Saidur, M. Samykano and V. Tyagi, *International Materials Reviews*, 2022, 1-44.
7. C. Booten, P. Rao, V. Rapp, R. Jackson and R. Prasher, *Joule*, 2021, **5**, 24-46.
8. Z. Said, A. A. Hachicha, S. Aberoumand, B. A. Yousef, E. T. Sayed and E. Bellos, *Progress in Energy and Combustion science*, 2021, **84**, 100898.
9. M. George, A. Pandey, N. Abd Rahim, V. Tyagi, S. Shahabuddin and R. Saidur, *Energy Conversion and Management*, 2019, **186**, 15-41.
10. Y. Peng and Y. Cui, *Joule*, 2020, **4**, 724-742.
11. X. Hu, Y. Zheng, D. A. Howey, H. Perez, A. Foley and M. Pecht, *Progress in Energy and Combustion Science*, 2020, **77**, 100806.
12. L. Yang, J.-n. Huang and F. Zhou, *Energy conversion and management*, 2020, **214**, 112876.
13. E. Alehosseini and S. M. Jafari, *Trends in Food Science & Technology*, 2019, **91**, 116-128.
14. A. Pandey, M. Hossain, V. Tyagi, N. Abd Rahim, A. Jeyraj, L. Selvaraj and A. Sari, *Renewable and Sustainable Energy Reviews*, 2018, **82**, 281-323.
15. P. Cheng, X. Chen, H. Gao, X. Zhang, Z. Tang, A. Li and G. Wang, *Nano Energy*, 2021, **85**, 105948.
16. S. Harikrishnan, M. Deenadhayalan and S. Kalaiselvam, *Energy Conversion and Management*, 2014, **86**, 864-872.
17. Z. Tang, Y. Gao, P. Cheng, Y. Jiang, J. Xu, X. Chen, A. Li and G. Wang, *Nano Energy*, 2022, 107383.
18. J. Wang, H. Xie, Z. Guo, L. Guan and Y. Li, *Applied Thermal Engineering*, 2014, **73**, 1541-1547.
19. W. Cui, X. Li, X. Li, L. Lu, T. Ma and Q. Wang, *Applied Energy*, 2022, **309**, 118465.
20. X. Wu, M. Gao, K. Wang, Q. Wang, C. Cheng, Y. Zhu, F. Zhang and Q. Zhang, *Journal of Energy Storage*, 2021, **36**, 102398.
21. Y. Li, S. Yu, P. Chen, R. Rojas, A. Hajian and L. Berglund, *Nano Energy*, 2017, **34**, 541-548.
22. S. Wu, T. Yan, Z. Kuai and W. Pan, *Energy Storage Materials*, 2020, **25**, 251-295.
23. B. Xu, B. Wang, C. Zhang and J. Zhou, *Thermochimica Acta*, 2017, **652**, 77-84.
24. M. F. El-Kady, Y. Shao and R. B. Kaner, *Nature Reviews Materials*, 2016, **1**, 1-14.
25. F. Wang, J. Liu, X. Fang and Z. Zhang, *Solar Energy Materials and Solar Cells*, 2016, **147**, 101-107.

26. T. Li, M. Wu, S. Wu, S. Xiang, J. Xu, J. Chao, T. Yan, T. Deng and R. Wang, *Nano Energy*, 2021, **89**, 106338.
27. T.-H. Wang, T.-F. Yang, C.-H. Kao, W.-M. Yan and M. Ghalambaz, *Advanced Powder Technology*, 2020, **31**, 2421-2429.
28. Y. Wang, F. Wang, L. Zhao, Z. Mao, X. Feng, X. Sui and B. Wang, *Chemical Engineering Journal*, 2022, **431**, 133983.
29. Y. Liu, R. Zheng, T. Tian and J. Li, *Energy Conversion and Management*, 2022, **267**, 115902.
30. I. Daou, L. El-Kaddadi, O. Zegaoui, M. Asbik and N. Zari, *Journal of Energy Storage*, 2018, **17**, 84-92.
31. K. Wang, T. Yan, Y. Zhao, G. Li and W. Pan, *Energy*, 2022, **242**, 122972.
32. N. Şahan and H. Paksoy, *Composites Part B: Engineering*, 2017, **126**, 88-93.
33. S. Dhivya, S. I. Hussain, S. J. Sheela and S. Kalaiselvam, *Thermochimica Acta*, 2019, **671**, 70-82.
34. Y. K. Mishra and R. Adelung, *Materials Today*, 2018, **21**, 631-651.
35. M. Hasanpoor, M. Aliofkhazraei and H. Delavari, *Ceramics International*, 2016, **42**, 6906-6913.
36. Y. K. Mishra, G. Modi, V. Cretu, V. Postica, O. Lupan, T. Reimer, I. Paulowicz, V. Hrkac, W. Benecke and L. Kienle, *ACS Applied Materials & Interfaces*, 2015, **7**, 14303-14316.
37. D. Gedamu, I. Paulowicz, S. Kaps, O. Lupan, S. Wille, G. Haidarschin, Y. K. Mishra and R. Adelung, *Advanced Materials*, 2014, **26**, 1473-1473.
38. F. H. Alsultany, Z. Hassan and N. M. Ahmed, *Sensors and Actuators A: Physical*, 2016, **250**, 187-194.
39. P. Steurer, R. Wissert, R. Thomann and R. Mülhaupt, *Macromolecular Rapid Communications*, 2009, **30**, 316-327.
40. J. L. Cheong, C. Hu, W. Liu, M.-F. Ng, M. B. Sullivan and J. Y. Ying, *Nano Energy*, 2022, 107659.
41. G. Fang, Z. Chen and H. Li, *Chemical Engineering Journal*, 2010, **163**, 154-159.
42. D. L. Pavia, G. M. Lampman, G. S. Kriz and J. A. Vyvyan, *Introduction to spectroscopy*, Cengage learning, 2014.
43. S. Ramakrishnan, X. Wang, J. Sanjayan, E. Petinakis and J. Wilson, *Solar Energy*, 2017, **158**, 626-635.
44. B. Kalidasan, A. Pandey, S. Shahabuddin, M. George, K. Sharma, M. Samykano, V. Tyagi and R. Saidur, *Renewable Energy*, 2021, **173**, 1057-1069.
45. C. Latha, M. Raghasudha, Y. Aparna, D. Ravinder, P. Veerasomaiah and D. Shridhar, *Materials Research*, 2017, **20**, 256-263.
46. C. Parkinson and E. Wollack, *NASA, Winner*, 2010, **22**.
47. V. Postica, I. Paulowicz, O. Lupan, F. Schütt, N. Wolff, A. Cojocaru, Y. K. Mishra, L. Kienle and R. Adelung, *Vacuum*, 2019, **166**, 393-398.
48. B. Kalidasan, A. Pandey, S. Rahman, A. Yadav, M. Samykano and V. Tyagi, *Sustainability*, 2022, **14**, 13240.
49. A. K. Mishra, B. B. Lahiri and J. Philip, *ACS Omega*, 2018, **3**, 9487-9504.
50. J. K. Carson, S. J. Lovatt, D. J. Tanner and A. C. Cleland, *International Journal of Heat and Mass Transfer*, 2005, **48**, 2150-2158.
51. X. Yang, C. Liang, T. Ma, Y. Guo, J. Kong, J. Gu, M. Chen and J. Zhu, *Advanced Composites and Hybrid Materials*, 2018, **1**, 207-230.
52. Y. Zhou, X. Wang, X. Liu, D. Sheng, F. Ji, L. Dong, S. Xu, H. Wu and Y. Yang, *Solar Energy Materials and Solar Cells*, 2019, **193**, 13-21.

53. L. Colla, L. Fedele, S. Mancin, L. Danza and O. Manca, *Applied Thermal Engineering*, 2017, **110**, 584-589.

Declaration of interests

☒ The authors declare that they have no known competing financial interests or personal relationships that could have appeared to influence the work reported in this paper.

☐The authors declare the following financial interests/personal relationships which may be considered as potential competing interests: